^{4}He adsorbed in cylindrical silica nanopores: Effect of size on the single-atom mean kinetic energy

C. Andreani,[1,2] C. Pantalei,[1] and R. Senesi[1,2]
[1]*Dipartimento di Fisica, Università degli Studi di Roma "Tor Vergata," Via della Ricerca Scientifica 1, 00133 Roma, Italy*
[2]*NAST, Centro di Nanoscienze, Nanotecnologie, Strumentazione, Università degli Studi di Roma "Tor Vergata," Via della Ricerca Scientifica 1, 00133 Roma, Italy*

(Received 9 October 2006; revised manuscript received 5 January 2007; published 28 February 2007)

This paper reports a study of the short-time dynamics of helium confined in silica nanopores (xerogel powder), with average pore diameters of 24 and 160 Å. The longitudinal momentum distribution of helium adsorbed in xerogels has been determined via deep inelastic neutron scattering (DINS) measurements performed on the VESUVIO spectrometer at the ISIS spallation source. DINS measurements, in the attosecond time scale, (i.e., 10^{-16}–10^{-15} s), were performed at a temperature of $T=2.5$ K and saturated vapor pressure conditions, with 95% pore volume filling. The average wave-vector transfer q was about 130 Å^{-1}. For confined helium, significant changes in the values of the single-particle mean kinetic energies $\langle E_K \rangle$ are found in the bulk phase. These are 32.6 ± 8.7 K for the 24 Å and 24.4 ± 5.3 K for the 160 Å pore diameters, remarkably higher than $\langle E_K \rangle = 16.2 \pm 0.4$ K, the value of normal liquid ^{4}He at $T=2.5$ K and saturated vapor pressure conditions. The results are interpreted in terms of a model where ^{4}He atoms are arranged in concentric annuli along the cylindrical pore axis, with $\langle E_K \rangle$ mainly dependent on the ratio between the atomic "effective" diameter and the pore diameter. The number of solid layers close to pore surface is found to be strongly pore-size dependent with one single solid layer for 24 Å diameter pore and three solid layers for 160 Å diameter pore.

DOI: 10.1103/PhysRevB.75.064515 PACS number(s): 61.12.−q, 67.20.+k, 61.43.Gt

I. INTRODUCTION

It is well known that static and dynamical microscopic properties of fluids adsorbed in nanoporous materials significantly differ from those in the bulk phase.[1,2] The confining geometry and the enhanced surface interaction due to the large surface-to-volume ratio of porous materials modify liquid-vapor and liquid-solid transitions. When atomic and molecular systems are adsorbed in nanometric pores, they experience a reduction in the number of nearest neighbors, with effects on microscopic properties as well as on phase diagram.[3] For slit-shaped pores, such as in carbon fibers, reduction of the pore width affects the confined system, inducing change from a nearly three-dimensional to a two-dimensional behavior. For cylindrical geometries, reduction in pore diameter leads to one- and quasi-one-dimensional behavior.[4]

Spectroscopic studies of organic molecules in silica xerogel matrices, of different pore sizes, have shown marked effects on the dynamics of the host molecules due to the confinement induced by the surrounding silica cages.[5] In the case of quantum systems such as ^{4}He, the interplay between the small atomic mass and geometry of the confining volumes results in a broadening of the single-particle momentum distribution $n(p)$ with an increase of the single-particle kinetic energy $\langle E_K \rangle$ values and at the same time an enhancement of the Bose-Einstein condensate fraction.[1,6] ^{4}He films adsorbed in pores with diameter larger than 50 Å show a superfluid transition through a size-dependent Kosterlitz-Thouless transition.[7] Since the experimental value of the vortex core size is 25 ± 12 Å, the pore size is crucial for the determination of superfluid transition temperature. In particular, for pore diameter of approximately 25 Å, torsional oscillator measurements indicate that no superfluid behavior shows up for pore coverage below 1.25 atomic layers.[8] As coverage increases to full pore fillings, a superfluid film grows on the nonsuperfluid layers. Furthermore, upon increasing pressure up to a critical pressure $P_c \simeq 3.4$ MPa, a phase transition develops from a superfluid to a nonsuperfluid phase.[8]

Neutron-scattering measurements performed on liquid ^{4}He, confined in MCM-41 with 47 Å pore diameter, show that up to about 1.67 layers coverage, helium films are solidlike and do not show any low-dimensional liquid excitations.[9] At the same time, investigations by torsional oscillator measurements of ^{4}He film on mesoporous folded sheet mesoporous (FSM) silica substrates of 47 Å mean pore diameter indicate a superfluid film response above 1.5 atomic layer coverage.[10] Systematic studies of film formation, by vapor pressure measurements, have also been performed on He adsorbed in FSM silica substrates, with pore diameters ranging from 18 to 47 Å.[7] These studies demonstrated that the film growth shows no pore-size dependence, indicating that completion of this layer is primarily dominated by the He-silica van der Waals interaction.[7] On the other hand, film growth after the first layer completion shows a strong pore-size dependence. Neutron-diffraction measurements of helium films adsorbed on graphite made it possible to determine the microscopic structure of the first two solid layers at the liquid-solid boundary. The results suggest that the effect of the substrate-helium interaction extends to several layers above the first monolayer.[11] It appears that the exact nature of films above the first layer completion shows a marked pore-size dependence; the second- and third-layer ordering are strongly influenced by the surface corrugation and the detailed balance between He-substrate and He-He interactions. The microscopic structural and dynamical interpretation of these properties is the subject of experimental and

theoretical research activities. With this respect, we recall that a "persistent liquid-layer," i.e., a second liquidlike layer, interpretation of the supersolid phase transition of solid ^{4}He confined in Vycor nanopores is the subject of recent theoretical and experimental studies.[12–14]

The eV neutron spectroscopy provides valuable microscopic information on the effects of both surface interactions and confinement. Deep inelastic neutron scattering (DINS) is a unique technique to probe the short-scale dynamics, allowing us to directly determine the momentum distribution and mean kinetic energy of the confined atoms and molecules.[15,16] It provides an insight into single-particle potentials and wave functions, with a direct determination, in several cases, of the Born-Oppenheimer potential of the scattering particle.[15] Recent experimental DINS measurements of ^{4}He, adsorbed in flat surface or slit-geometry porous substrates, have shown a large increase in $\langle E_K \rangle$ and n_0, the condensate fraction of atoms with zero momentum.[1,6] This has been attributed to the strong localization effects induced by the helium-substrate interaction potential, which mainly influence the first two or three adsorbed layers.[6] At the same time, a reduction in the equilibrium pressure observed at low helium coverage has been attributed to a reduced local density of the adsorbate. The latter determines smaller interatomic interactions and, consequently, an enhancement on the formation of the condensate.[1] Other DINS measurements on liquid ^{4}He confined in Vycor (cylindrical pore geometry) have shown that, if scattering contribution from the first adsorption layers is subtracted, the adsorbed ^{4}He is in the liquid phase with values for both condensate fraction and kinetic energies similar to bulk phase.[17] In this context, it is interesting to study the effect on the dynamics of ^{4}He confined in cylindrical pore geometries due to pore size. In this case, theoretical predictions suggest that the corrugation experienced by atoms close to surface is much smaller than that on planar surface.[18] Studies of adsorption of helium on a variety of surfaces have provided a wealth of information on the behavior of low-dimensional quantum solids and their interaction with substrates.[19] While the most extensive studies of phase diagram and thermal properties of the first layers have been carried out on graphitic substrates, comparable extended studies on silica substrates and cylindrical geometry have not been performed.

This paper reports a study of the short-time dynamics of helium confined in nanoporous materials (silica xerogel powder) performed via DINS measurements on the VESUVIO spectrometer at the ISIS spallation neutron source.[15] The measurements were performed in the attosecond time scale (i.e., 10^{-16}–10^{-15} s). Aims of this work were to determine single-particle mean kinetic energy $\langle E_K \rangle$ of ^{4}He adsorbed in cylindrical silica nanopores for two different pore diameters, namely, 24 and 160 Å, and to study the dependence of single-particle dynamics on pore sizes, layer coverage, and geometry of the confining system. A 24 Å pore diameter corresponds to approximately ten times the Lennard-Jones hard-core diameter, i.e., σ_d=2.556 Å,[20] and a 160 Å pore diameter is about 60 times σ_d. In the latter case, to a good approximation, the corrugation experienced by helium atoms close to nanoporous surface resembles that of a planar surface. An extrapolation to slit geometry is then applied to derive helium monolayer dynamical properties. Changes of the helium single-particle dynamics from values in bulk phase are found. Results are discussed in terms of the interaction of helium atoms with the silica substrate. It is shown that strongly localized layers, above the first one, clearly manifest in a DINS measurement, giving rise to an enhancement of the $\langle E_K \rangle$ values. These findings provide an insight into the inner layer ordering in porous matrices.

II. EXPERIMENT

The DINS measurements were carried out on the VESUVIO instrument, an inverse-geometry eV spectrometer operating at the ISIS pulsed neutron source (Chilton, Didcot, UK).[15] The neutron-scattering spectrum is reconstructed using the filter difference technique, where final energy is selected by resonant foil analyzers, placed between sample and detectors. Gold (^{197}Au) foil filters with resonant energy E_1 =4.908 eV were chosen for the present experiment. Scattered neutrons were detected, via the time-of-flight technique, by 88 glass scintillators (^{6}Li-enriched fixed-angle elements), covering an angular range $140° < 2\theta < 164°$. In the present experiment, only a subset of the total backscattering detector array was available, corresponding to a solid angle of approximately 0.31 sr. DINS spectra have been simultaneously recorded with analyzers of two different thicknesses thin (7 μm) and thick (21 μm), but, due to the detection solid angle limitations, no attempt has been made to record with the double difference acquisition mode.[21,22] The average wave-vector transfer q accessed in these measurements was $q \simeq 130$ Å^{-1}, corresponding to an average energy transfer $\hbar\omega$ of approximately $\hbar\omega \simeq 11$ eV. The SiO_2 xerogel powders can be synthesized with average pore size ranging between 10 and 160 Å, and surface areas ranging between 200 and 800 m^2/g depending on the synthesis procedures and on the postdeposition treatments. Acid or base catalytic synthesis, aging, condensation rates, and densification at high temperatures of the formed xerogel glasses are all parameters which strongly influence surface area, pore volume, and pore-size distribution of the samples. In the present experiment, SiO_2 xerogel powders with two different pore sizes, 24±7 Å (sample I) and 160±15 Å (sample II), have been synthesized following the procedures of Ref. 5. The xerogel powder confining samples had an approximate volume of 15 cm^3 and were vacuum pumped for 24 h at 60 °C. The nanoporous materials have been characterized by Brunauer-Emmet-Teller (BET) method[23] based on nitrogen adsorption-desorption isotherms. The porous properties of the two xerogel glasses are reported in Table I.

DINS measurements were performed on both ^{4}He adsorbed in xerogel powders and on the dry xerogel powders. Samples were placed in an Al slab container, with 5 mm internal thickness. All measurements were performed at a temperature T=2.5 K and saturated vapor pressure conditions. Two Ge resistance thermometers, located at the upper and lower ends of the sample cell, were employed for temperature control, with an average value T=(2.5±0.01) K throughout the measurements. An additional measurement on

TABLE I. Physical parameters of xerogel glasses as determined by BET method.

Sample	Pore diameter (Å)	Total pore volume (cm^3/g)	Specific surface area (m^2/g)
I	24	0.348	727
II	160	1.38	301

polycrystalline Pb sample has been carried out in order to calibrate the instrumental parameters (flight paths, angles, etc.) and derive the instrumental resolution function $R(y)$ [see Eq. (2.4) below].[15]

A run on each dried xerogel has been carried out first in order to record the recoil scattering contributions from Al, Si, and O. Two reservoirs of fluid ^{4}He were prepared at room temperature: with a volume of 4 l and a pressure $P=1133.0$ mbar (sample I, see Table I), and with a volume of 50 l at $P=130.2$ mbar (for sample II). These are the amounts, determined from the total pore volume (see Table I), corresponding to a 95% pore filling fraction in the xerogels, for both pore diameters. The two samples of ^{4}He confined in xerogel were prepared using a gas-handling rig by condensing the fluid, at $T=2.5$ K, from reservoirs into the cell. Pressures were controlled by a Baratron transducer placed on a capillary in the rig. After approximately 3 h, an equilibrium pressure was reached for both samples, with values $P_I=98.0$ mbar for sample I and $P_{II}=79.0$ mbar for sample II. These values are slightly lower than the saturated vapor pressure for bulk ^{4}He at 2.5 K, $P_0=100.0$ mbar.[24] Once equilibrium pressure was reached, the gas-handling rig was vacuum pumped to remove any excess helium not adsorbed in the xerogels. The experiment runs were performed with a pressure stability always within 2 mbar. DINS measurements were carried out for about 72 h for each sample. The filter difference technique guarantees that each recorded scattering spectrum contains no additional background contribution. This is removed by the *filter-in/filter-out* difference

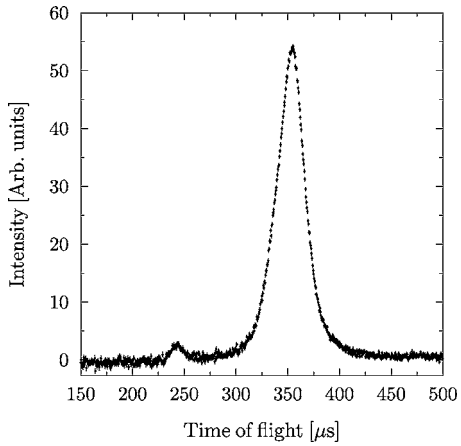

FIG. 1. Example of a time-of-flight DINS spectrum for sample II (see Table I). Data represent the sum of DINS signals collected from 15 detectors at fixed angles in the angular range $142° < 2\theta < 149°$. The peak at ~240 μs corresponds to recoil from ^{4}He; the peak at ~350 μs corresponds to recoil from O, Si, and Al masses.

procedure.[15] Fixed-angle spectra show the contributions of four recoil peaks, corresponding to DINS scattering from O, Si, Al, and ^{4}He components (see Fig. 1). From Fig. 1, one can note that the ^{4}He peak is well separated from other contributions.

Given the large values of q and $\hbar\omega$ of the present experiment, the DINS response function can be expressed within the framework of the *impulse approximation* (IA),[15] in terms of the *neutron Compton profile* (NCP), $J(y,\hat{q})$. The latter function represents the probability density distribution of y, i.e., the atomic momentum component along the direction of the wave-vector transfer $\hat{q}$. The quantity $y=\frac{M}{\hbar q}\left(\omega-\frac{\hbar q^2}{2M}\right)$ is the West scaling variable,[16,25] M is the atomic mass of the struck nucleus, and $\hbar\omega$ is the energy transfer. Within the IA, the dynamical structure factor $S_{\mathrm{IA}}(\mathbf{q},\omega)$ is expressed in terms of the response function

$$S_{\mathrm{IA}}(\mathbf{q},\omega)=\int n(\mathbf{p})\delta\left(\omega-\frac{\hbar q^2}{2M}-\frac{\mathbf{q}\cdot\mathbf{p}}{M}\right)d\mathbf{p}=\frac{M}{\hbar q}J(y,\hat{q}). \tag{2.1}$$

In an isotropic liquid, there is no dependence on the direction of the wave-vector transfer $\hat{q}$ and the response function becomes

$$J(y)=2\pi\hbar\int_{|\hbar y|}^{\infty}pn(p)dp. \tag{2.2}$$

Values of $\langle E_K\rangle$ are obtained from the second moment sum rule for $J(y)$,[16,26]

$$\int_{-\infty}^{\infty}y^2J(y)dy=\sigma^2=\frac{2M}{3\hbar^2}\langle E_K\rangle, \tag{2.3}$$

where σ is the standard deviation of the response function.

Deviations from the IA, generally described in terms of the *final state effects*, are negligible in the present (q,ω) range and do not affect significantly the recoil peak shapes.[15]

A different procedure has been developed in order to analyze the DINS data sets, for both thin- and thick-foil analyzers, of this experiment. Multiple scattering contributions have been evaluated by implementing the DINSMS simulation package[27] such as to include the energy transfer function for thick foil. The simulated spectra, and the corresponding multiple scattering contributions, were obtained for each individual fixed-angle detector element. The dry xerogel runs have been subtracted off both sample I and II runs in order to remove the signal coming from O, Al, and Si recoil peaks. The resulting time-of-flight spectra have then been transformed in the y space using standard VESUVIO routines[28] to yield the fixed-angle NCPs. In the framework of the convolution approximation, the individual NCPs at fixed angle are expressed by

$$F(y)=J(y)\otimes R(y). \tag{2.4}$$

The experimental resolution $R(y)$ has been determined through a simulation, employing the DINSMS code,[27] of the DINS spectra and a comparison with DINS experimental spectra from Pb (with $M=207$ amu). Parameters of the code have been varied until the simulated spectra provided a sat-

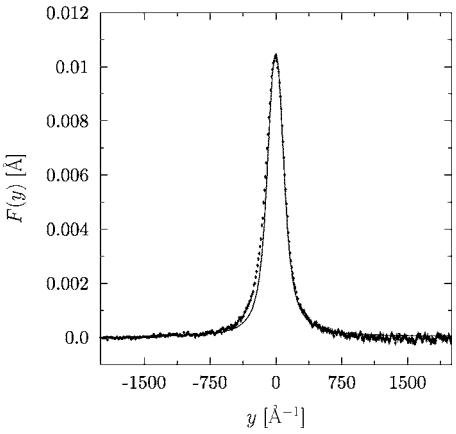

FIG. 2. Experimental neutron Compton profile (NCP) from polycrystalline Pb sample, measured with thick analyzers (circles with error bars); simulated data (continuous line). Data are the averaged sum over 44 detectors placed at fixed angles.

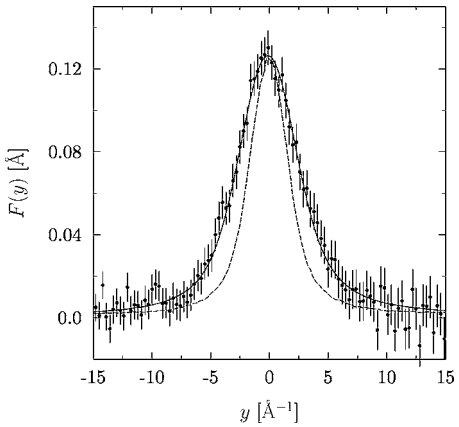

FIG. 3. Neutron Compton profile (NCP) for sample II, measured with thick analyzers (circles with error bar) and the corresponding best fit (continuous line); instrumental resolution function $R(y)$ (dashed line).

isfactory reproduction of the experimental spectra. A parameter of particular importance is the thickness of the analyzer foils, which determines the analyzer energy transfer functions. A comparison between simulated and experimental data is reported in Fig. 2 as an example.

A second simulation was carried out in order to determine the resolution in the ^{4}He momentum space. In this simulation, the spectrometer's response for ^{4}He mass was determined using the dynamical structure factor of Eq. (2.1) with $n(p) \rightarrow \delta(p)$, a procedure commonly employed in the case of DINS measurements.[29] The high value of wave-vector transfer available at each detector ($q \simeq 130$ Å^{-1}) allowed us to average the whole set of individual fixed-angle experimental and resolution spectra for each xerogel sample. Moreover, the present wave-vector transfer range guarantees that deviations from the impulse approximation, referred to as final state effect contributions, were negligible.[15] A single response function and the corresponding resolution were then obtained. A model line-shape function employed for the NCP analysis is a Gaussian of the following form:

$$J(y) = \frac{1}{\sqrt{2\pi\sigma^2}} \exp\left(-\frac{y^2}{2\sigma^2}\right), \tag{2.5}$$

where σ is the standard deviation of the NCP. The current data were satisfactorily fitted with the single parameter σ, and no higher-order non-Gaussian terms[30] were required. The line-shape analysis of the experimental NCP was carried out for each xerogel sample by performing a simultaneous fit of the thin-foil and thick-foil spectra, using in Eq. (2.4) the model function of Eq. (2.5). Figure 3 reports an example of the NCP line shape for sample II, with the corresponding best fit. The resulting kinetic energies, derived from the values of σ for samples I and II, are reported in Table II.

III. RESULTS AND DISCUSSION

Results listed in Table II indicate that for both samples, values of $\langle E_K \rangle$ greatly exceed the value at equilibrium pressure of normal liquid ^{4}He, namely, $\sim$16 K.[31] This finding is in agreement with previous determinations of mean kinetic energy of ^{4}He adsorbed in porous graphite and MgO.[1,6] Moreover, the $\langle E_K \rangle$ increases as the pore diameter is reduced. This is interpreted by considering that the experimental $\langle E_K \rangle$ values of Table II are average signals among helium atoms localized either in the bulk of the pores or close to the surface of the pores. It has to be noted that helium atoms adsorbed within the first layer experience a great localization due to the resulting ^{4}He-surface potential with an attractive well of about −153 K, an order of magnitude larger than the helium-helium interaction attractive well.[20] Therefore, for helium atoms closer to the pore surface, a higher value of $\langle E_K \rangle$ is expected as compared to helium atoms within the bulk of the pores. In support of this picture are also results of a recent theoretical study of the microscopic structure and dynamics of ^{4}He, confined in a cylindrical geometry silica matrix with 26 Å pore diameter,[32] i.e., a confining geometry very similar to sample I of the present experiment. The authors suggest that helium atoms are arranged in concentric annuli along the pore axis: the first atomic layer experiences a great localization, whereas atoms in the second and inner adsorption layers are found in the liquid phase, at a density value ρ=0.0240 Å^{-3}. The latter is very close to the value of density of the present experiment, ρ=0.0218 Å^{-3}. By increasing pressure, i.e., helium density in the pores, this study also predicted that a solidification process occurs with the progressive involvement of inner layers.[32]

Let us then assume that the $\langle E_K \rangle$ value for sample I (see Table II) results from a distribution of kinetic-energy values

TABLE II. Single-particle mean kinetic energies for samples I and II. The value for normal liquid ^{4}He at T=2.5 K is from Ref. 31.

Sample	Pore diameter (Å)	$\langle E_K \rangle$ (K)	Filling fraction (%)
I	24	32.6±8.7	95
II	160	24.4±5.3	95
Bulk liquid ^{4}He		16.2±0.4	

associated with atoms belonging to a highly localized solidlike layer, $\langle E_K\rangle_s$, and to inner liquidlike layers, $\langle E_K\rangle_l$. Given the cylindrical symmetry of the confining system, one can express $\langle E_K\rangle$ in terms of two distinct contributions, the solidlike layers and the inner liquidlike layers, via the following model:[33]

$$\langle E_K\rangle = \frac{N\langle E_K\rangle_s + (N_{tot}-N)\langle E_K\rangle_l}{N_{tot}}, \tag{3.1}$$

where N is the number of atoms of solidlike layers (one in the present case) and N_{tot} is the total number of atoms in the liquid layers in a circular section along the pore axis. N has been determined by considering the arrangement of atoms, of effective diameter σ_d=2.556 Å, in a concentric annulus of thickness σ_d and external diameter d=24 Å. Similarly, N_{tot} has been determined by summing the contributions from the first and inner layer concentric annuli, taking into account the 95% volume filling fraction. It has to be stressed that the important parameter in this model is the ratio σ_d/d. This results in a ratio between the number of atoms in solid and liquid layers, $f(\mathrm{I})=N/N_{tot}=0.39$, with a coverage of four concentric annular layers, in agreement with the theoretical estimates of the radial density profiles of Ref. 32. It is clear from Eq. (3.1) that $\langle E_K\rangle$ depends linearly on f. From the value of $\langle E_K\rangle$ and Eq. (3.1), it is thus possible to obtain an estimate of the monolayer single-particle kinetic energy, $\langle E_K\rangle_s$=58.5±15 K. This value compares very well with the value $\langle E_K\rangle$=55.8±4.5 K found for ^{4}He adsorbed on activated carbon fibers at 4.6 K,[6] the latter system being characterized by a slit geometry with a slit width of the order of 6 Å and a single-layer ^{4}He coverage.

The same approach, assuming a single solid layer close to pore surface has been employed for sample II, where $f(II)=N/N_{tot}=0.065$: in this case the corresponding calculated value of $\langle E_K\rangle$ is 18.8±1.9 K, i.e., lower than the experimentally determined value (see Table II). However, one has to bear in mind that, for large diameter pores, surface roughness needs to be accounted for.[18] The latter may induce higher localization effects on inner layers as well. In this context, recent inelastic neutron scattering measurements performed on helium adsorbed in 133 Å diameter silica xerogels, suggest that two to three solidlike adsorption layers may be present.[34]

The present result of more than a single solidlike layer for the large pore xerogel are also relevant for the connection with studies of the superfluid response of pressurized ^{4}He in nanoporous confinement. In particular, recent neutron diffraction measurements of solid ^{4}He in 70 Å diameter silica pores suggest that crystallization is incomplete, i.e., about 70% of the pore filling is noncrystalline.[35] The noncrystalline fraction presumably consists of about two monolayers of "immobile" atoms close to the pore walls and a liquidlike shell between this wall coating and the crystalline core in the pore centers.[35] In the present model, the layers of immobile (highly localized) atoms contribute, see Eq. (3.1), to the mean kinetic energy with the same single-particle value, $\langle E_K\rangle_s$.

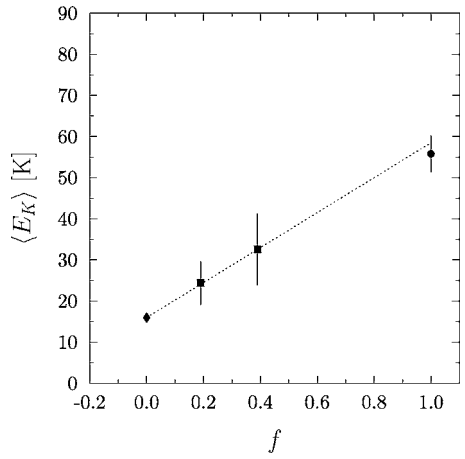

FIG. 4. Single-atom mean kinetic energies as a function of the ratio between the number of atoms in solid and liquid layers, $f=N/N_{tot}$. Present experiment, squares. Experimental bulk liquid value from Ref. 31, diamond. Experimental value of $\langle E_K\rangle$ for helium adsorbed in active carbon fibers, i.e., monolayer coverage, $f=1$, and slit geometry from Ref. 6 (circle). Model determined from Eq. (3.1), dotted line. The three experimental values for confined helium correspond to a transition from planar (160 Å pore diameter) to cylindrical (24 Å pore diameter) to slit (activated carbon fibers) geometries.

Within the latter assumption, if one assigns a value of $\langle E_K\rangle_s$=58.5±15 K to the first three layers of sample II, then one finds $f(\mathrm{II},3\ \mathrm{layers})=N/N_{tot}=0.19$ and calculates [from Eq. (3.1)] $\langle E_K\rangle$=23.9±1.9 K. This value is in very good agreement with the present DINS experiment. The experimental determinations of $\langle E_K\rangle$ and the corresponding calculated values of Eq. (3.1) are reported, for the two samples, in Fig. 4. Although the model implies an uncorrelated sum of contributions from liquidlike and solidlike layers, the value of $\langle E_K\rangle$ for monolayer coverage is found to be in very good agreement with independent experimental results. The experimental value for sample II indicates that more than a single layer is highly localized and solidlike, as suggested in Ref. 34, and that good agreement with the measured kinetic energy is reached for three solid layers. These results suggest that the inner layer ordering in porous matrices depends on pore size and, upon approaching a planar geometry, higher localization on inner layers is promoted.

IV. CONCLUSIONS

The single-particle mean kinetic energies $\langle E_K\rangle$ of ^{4}He adsorbed (95% filling) in silica nanopores of 24 and 160 Å mean pore diameters have been measured at 2.5 K and equilibrium pressure. These pore sizes guaranteed that the geometry of the nanoporous materials (xerogel powders) closely resembles a cylindrical and an almost planar confinement, respectively. The single-particle dynamics of confined helium atoms is shown to be significantly affected by confinement and its dependence is discussed in terms of pore sizes, layer coverage, and geometry of the confining system. Values of $\langle E_K\rangle$ of helium adsorbed in xerogel powders are found

significantly higher than those in bulk liquid.[1,6] The mean kinetic energy increases by reducing the pore size. This behavior is described within a microscopic structural model, where the adsorption of atoms occurs through atomic layers formed from the pore surfaces. In this model, ^{4}He atoms are assumed to be arranged in concentric annuli along the cylindrical pore axis, with the number of atoms in each layer depending on the ratio of the atomic "effective" diameter to the pore diameter. The resulting mean kinetic-energy values are interpreted within a model of uncorrelated sum of contributions ranging from inner liquidlike layers to the solidlike layers close to the pore surface.[33] In the case of ^{4}He adsorbed in pores of 24 Å diameter (sample I), the experimental mean kinetic-energy value is well reproduced by assuming a single layer, solidlike, with all other inner layers in the liquid phase. The extrapolated value of the first layer close to pore surface corresponds to a high value of kinetic energy ($\langle E_K \rangle_s = 58.5 \pm 15$ K). For the ^{4}He adsorbed in pores of 160 Å diameter (sample II), the surface roughness plays a relevant role and the result is interpreted in terms of three layers, solidlike, with the same high kinetic energy ($\langle E_K \rangle_s = 58.5 \pm 15$ K) as found in smaller pore diameter. In this case, the pore diameter is about 60 times the hard-core Lennard-Jones diameter; thus, the nanoporous confinement approaches a planar geometry. For both samples of helium atoms adsorbed in xerogel powder, the remaining inner layers are found in the liquid phase.

In conclusion, this work shows that values of helium mean kinetic energy are significantly affected by confinement size as well as surface geometry. Confinement induced changes result in higher values of $\langle E_K \rangle$ than those in bulk liquid and a variable number of highly localized layers.

Further DINS measurements in ^{4}He confined in organic/inorganic matrices of different pore diameters and geometries are planned in order to derive a comprehensive picture of the single-particle short-time dynamics of helium in nanometric confinement.

ACKNOWLEDGMENTS

This work was supported within the CNR-CCLRC Agreement No. 01/9001 concerning collaboration in scientific research at the spallation neutron source ISIS. The financial support of the Consiglio Nazionale delle Ricerche in this research is hereby acknowledged. The authors acknowledge M. Casalboni, S. Dirè, P. Prosposito, and S. Schutzmann for their support in the synthesis process and characterization of the xerogel samples.

[1] J. V. Pearce, S. O. Diallo, H. R. Glyde, R. T. Azuah, T. Arnold, and J. Z. Larese, J. Phys.: Condens. Matter **16**, 4391 (2004).
[2] J. V. Pearce, M. A. Adams, O. E. Vilches, M. R. Johnson, and H. R. Glyde, Phys. Rev. Lett. **95**, 185302 (2005).
[3] L. Gelb, K. E. Gubbins, R. Radhakrishnan, and M. Sliwinska-Bartkowiak, Rep. Prog. Phys. **62**, 1573 (1999).
[4] J. Taniguchi, A. Yamaguchi, H. Ishimoto, H. Ikegami, T. Matsushita, N. Wada, S. M. Gatica, M. W. Cole, F. Ancilotto, S. Inagaki, and Y. Fukushima, Phys. Rev. Lett. **94**, 065301 (2005).
[5] M. Casalboni, R. Senesi, P. Prosposito, F. D. Matteis, and R. Pizzoferrato, Appl. Phys. Lett. **70**, 2969 (1997).
[6] D. Nemirovsky, R. Moreh, K. H. Andersen, and J. Mayers, J. Phys.: Condens. Matter **11**, 6653 (1999).
[7] H. Ikegami, T. Okuno, Y. Yamato, J. Taniguchi, N. Wada, S. Inagaki, and Y. Fukushima, Phys. Rev. B **68**, 092501 (2003).
[8] K. Yamamoto, H. Nakashima, Y. Shibayama, and K. Shirahama, Phys. Rev. Lett. **93**, 075302 (2004).
[9] F. Albergamo, J. Bossy, P. Averbuch, H. Schober, and H. R. Glyde, Phys. Rev. Lett. **92**, 235301 (2004).
[10] Y. Yamato, H. Ikegami, T. Okuno, J. Taniguchi, and N. Wada, Physica B **329**, 284 (2003).
[11] K. Carneiro, L. Passell, W. Thomlinson, and H. Taub, Phys. Rev. B **24**, 1170 (1981).
[12] J. Day, T. Herman, and J. Beamish, Phys. Rev. Lett. **95**, 035301 (2005).
[13] S. A. Khairallah and D. M. Ceperley, Phys. Rev. Lett. **95**, 185301 (2005).
[14] J. Day and J. Beamish, Phys. Rev. Lett. **96**, 105304 (2006).
[15] C. Andreani, D. Colognesi, J. Mayers, G. F. Reiter, and R. Senesi, Adv. Phys. **54**, 377 (2005).
[16] G. I. Watson, J. Phys.: Condens. Matter **8**, 5955 (1996).
[17] R. T. Azuah, H. R. Glyde, R. Scherm, N. Mulders, and B. Fåk, J. Low Temp. Phys. **130**, 557 (2003).
[18] G. Stan and M. W. Cole, Surf. Sci. **395**, 280 (1998).
[19] E. R. Dobbs, *Helium Three* (Oxford University Press, Oxford, 2000).
[20] R. A. Aziz, V. P. S. Nain, J. S. Carley, W. L. Taylor, and G. T. McConville, J. Chem. Phys. **70**, 4330 (1979).
[21] C. Andreani, D. Colognesi, E. Degiorgi, A. Filabozzi, M. Nardone, E. Pace, A. Pietropaolo, and R. Senesi, Nucl. Instrum. Methods Phys. Res. A **497**, 535 (2003).
[22] S. Imberti, C. Andreani, V. Garbuio, G. Gorini, A. Pietropaolo, R. Senesi, and M. Tardocchi, Nucl. Instrum. Methods Phys. Res. A **552**, 463 (2005).
[23] S. Brunauer, P. H. Emmett, and E. Teller, J. Am. Chem. Soc. **60**, 309 (1938).
[24] E. W. Lemmon, M. O. McLinden, and D. G. Friend, *Thermophysical Properties of Fluid Systems—NIST Standard Reference Database 69* (National Institute of Standards and Technology, Gaithersburg, MD, 2003).
[25] R. N. Silver and P. E. Sokol, *Momentum Distributions* (Plenum, New York, 1989).
[26] H. R. Glyde, *Excitations in Liquid and Solid Helium* (Clarendon, Oxford, 1994).
[27] J. Mayers, A. L. Fielding, and R. Senesi, Nucl. Instrum. Methods Phys. Res. A **481**, 454 (2002).
[28] R. Senesi, C. Andreani, A. L. Fielding, J. Mayers, and W. G. Stirling, Phys. Rev. B **68**, 214522 (2003).
[29] R. C. Blasdell and R. O. Simmons, Nucl. Instrum. Methods Phys. Res. A **405**, 71 (1998).
[30] C. Andreani, C. Pantalei, and R. Senesi, J. Phys.: Condens. Matter **18**, 5587 (2006).

[31] J. Mayers, C. Andreani, and D. Colognesi, J. Phys.: Condens. Matter **9**, 10639 (1997).
[32] M. Rossi, D. E. Galli, and L. Reatto, Phys. Rev. B **72**, 064516 (2005).
[33] D. Narehood, N. Grube, R. M. Dimeo, D. Brown, and P. Sokol, J. Low Temp. Phys. **132**, 223 (2003).
[34] C. R. Anderson, K. H. Andersen, W. G. Stirling, P. E. Sokol, and R. M. Dimeo, Phys. Rev. B **65**, 174509 (2002).
[35] D. Wallacher, M. Rheinstaedter, T. Hansen, and K. Knorr, J. Low Temp. Phys. **138**, 1013 (2005).